Journal of Materials Chemistry C

Accepted Manuscript

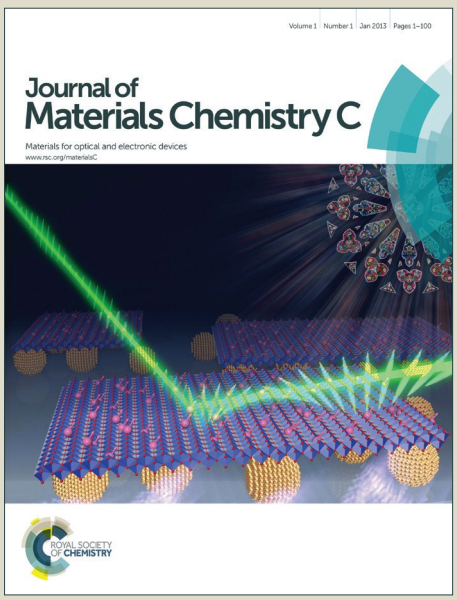

ROYAL SOCIETY OF CHEMISTRY

www.rsc.org/materialsC

Multiferroic properties and magnetoelectric coupling in Fe/Co co-doped $Bi_{3.25}La_{0.75}Ti_3O_{12}$ ceramics†

Ruixia Ti,[a] Xiaomei Lu,[*a,b] Ju He,[a] Fengzhen Huang,[a,b] Huarui Wu,[a] Fang Mei,[a] Min Zhou,[a] Yang Li,[a] Tingting Xu,[a] and Jinsong Zhu[a,b]

Polycrystalline $Bi_{3.25}La_{0.75}(Ti_{3-x}Fe_{x/2}Co_{x/2})O_{12}$ ($0 \le x \le 0.5$) ceramics are synthesized by conventional solid state reaction method. Good ferroelectricity and weak ferromagnetism are obtained simultaneously at room temperature when $x \ge 0.2$. The ceramics with $x = 0.25$ possess the best comprehensive properties, including high phase purity, large ferroelectric polarization, great dielectric constant, and also, larger remnant magnetization compared with other samples. Furthermore, significant dielectric anomalies appear near both the ferromagnetic Curie temperature and the spin glass freezing temperature. The possible magnetoelectric coupling mechanism is considered to be the associated binding effect of magnetic interaction on the migration of charged defects, especially oxygen vacancies.

1. Introduction

Multiferroic materials simultaneously exhibit ferroelectric and magnetic orders, and the coupling between two ferroic orders provides an additional degree of freedom in the design of novel multifunctional devices,[1] thus they have potential applications in information storage, spintronics, sensors, and so on.[2-4] However, most single-phase materials exhibit multiferroic properties at lower temperature, and the large difference between the magnetic and ferroelectric transition temperatures is clearly one of the obstacles to the exploitation of multiferroics in real applications. Various attempts have been made to synthesize room temperature multiferroic materials, among which doping magnetic species into ferroelectric materials is probably one of the most effective ways.[5-17] Ferromagnetism is successfully introduced into $BaTiO_3$ and $PbTiO_3$, conventional ferroelectric materials with simple perovskite structure, by doping magnetic ions (such as Fe or Mn) at the Ti-sites, however, the ferroelectricity is suppressed simultaneously due to the decreased structural distortion and the enhanced leakage current.[5-10] Recently, the multilayer-structured $Bi_{4+n}Ti_3Fe_nO_{12+3n}$, viewed as atomic stacking of a three-layered $Bi_4Ti_3O_{12}$ (BIT, ferroelectrics) and n layer perovskite $BiFeO_3$ (ferroelectric and antiferromagnetic at room temperature), has attracted great attention.[11-17] In this material system, the most widely investigated $Bi_5Ti_3FeO_{15}$ (BTF, n = 1) exhibits ferroelectricity, ferromagnetism and the coupling between them at room temperature,[11,12] and both the ferroelectricity and ferromagnetism are effectively strengthened through co-substituting with multi-elements and at multi-sites.[15,16] Actually, the Bi-layered BIT itself, especially $Bi_{3.25}La_{0.75}Ti_3O_{12}$ (BLT, BIT doped by La at the Bi-sites), is an important ferroelectric material for its high-performance, large polarization, and lead and fatigue-free characters.[18-21] Thus it is naturally expected to realize multiferroic properties and magnetoelectric coupling by doping magnetic ions into BLT. Currently, the limited related investigations mainly focus on BIT,[22-25] doping Nd/Sm at the Bi-sites and Fe/Co at the Ti-sites etc., and problems such as large leakage current, poor ferroelectricity and weak ferromagnetism are encountered. Meanwhile, Fe/Co co-substitution could enhance the magnetism because of the possible Fe-O-Co coupling,[24] which is also observed for the wildly investigated $Bi_5Ti_3FeO_{15}$ compound.[15,16] Therefore in our paper, the BLT ceramics co-doped by Fe and Co at the Ti-sites are fabricated, the coexistence of good ferroelectricity and weak ferromagnetism at room temperature is realized, and the sign of magnetoelectric coupling is also observed.

2. Experimental

Polycrystalline $Bi_{3.25}La_{0.75}(Ti_{3-x}Fe_{x/2}Co_{x/2})O_{12}$ (BLTFC) ($0 \le x \le 0.5$) ceramics were prepared by conventional solid state reaction method from high purity starting materials, including Bi_2O_3, La_2O_3, TiO_2, Fe_2O_3 and Co_2O_3. The ground and well mixed powders were preheated at 850 °C for 6 h, then ground, pressed into pellets under the pressure of 20 MPa, and sintered at 950 to 1050 °C for 6 h in air. Platinum electrodes

[a] National Laboratory of Solid State Microstructures and Physics School, Nanjing University, Nanjing 210093, People's Republic of China. E-mail: xiaomeil@nju.edu.cn

[b] Collaborative Innovation Center of Advanced Microstructures, Nanjing University, Nanjing 210093, People's Republic of China.

† Electronic Supplementary Information (ESI).

were sputtered on both sides of the samples for electrical measurements. X-ray diffraction (XRD, Bruker D8) with Cu Kα radiation, scanning electron microscopy (SEM, 1530YP) and Raman scattering spectra (Renishaw inVia Raman Microscope) were used for analyzing the microstructure of the samples. The dielectric properties were evaluated using a HP4194A impedance analyzer. The ferroelectric hysteresis loops and leakage current were measured by a TF2000 standard ferroelectric test unit, and magnetic properties were characterized by a commercial magnetic property measurement system (SQUID VSM, Quantum Design).

3. Results and discussion

From inset I of Fig. 1(a), the surface morphologies of BLTFC ceramics, it can be seen that the grain sizes of the doped ceramics decrease obviously compared with those of the un-doped ones. Figure 1(a), the XRD patterns of the samples, shows that the ceramics exhibit layered-perovskite structure, and most of the diffraction peaks can be indexed on the basis of orthorhombic cell.[26] The weak impurity peaks denoted by # and * belong to $Bi_2Ti_2O_7$ (for x = 0.1) and Bi_2O_3 (for x = 0.5), respectively, which should be related to the evaporation of Bi during high temperature sintering process and the non-stoichiometry induced by doping. None of the observable XRD peaks can be attributed to Fe/Co oxides and $CoFe_2O_4$. Inset II of Fig. 1(a) gives the amplified plot of the main diffraction peak (117), which shifts towards larger angles with increasing doping content due to the smaller radius of Fe^{3+} (0.550 Å) and Co^{3+} (0.545 Å) than that of Ti^{4+} (0.559 Å).[27] As shown by XPS spectra (ESI Fig. S1),† more oxygen vacancies present in the doped samples, indicating that Fe and Co ions mainly exist in low-valence state for charge balance, similar to other multilayered materials.[17,24] The crystal structure of BLTFC ceramics are refined (the reliability is ensured by the small parameters R_p and R_{wp}) based on orthorhombic space group $B2cb$ from Rietveld analysis using the General Structure Analysis System (GSAS) program pocket, and the refined parameters are summarized in Fig. 1(b). The unit cell volume V decreases with increasing doping content, consistent with the shift of the main diffraction peak (117), which indicates the lattice distortion in the doped ceramics.

Raman scattering was used to further examine the influences of Fe/Co doping on the BLT lattice. As shown in Fig. 1(c), the low frequency modes around 105, 125, and 155 cm^{-1} are ascribed to the vibration of Bi^{3+} ions in the perovskite layer, while the high frequency modes around 269, 343, 557, 625, and 851 cm^{-1} are attributed to the stretching and bending of the TiO_6 octahedra.[20,28,29] It can be seen that, after doping, although the above basic vibration modes remain, the relative intensity of them decreases with increasing doping content. Moreover, the Raman peaks around 269, 557, and 851 cm^{-1} become slightly broader, and that around 557 cm^{-1} moves a bit to higher frequencies, which are probably related to the lattice distortion and the stress caused by doping. In particular, a new vibration mode near 732 cm^{-1} arises with the intensity increasing with doping content, which doesn't belong to Fe/Co oxides and $CoFe_2O_4$,[30-32] but possibly associated with the FeO_6 and CoO_6 octahedra.[14,15] All these results indicate that Fe and Co ions successfully enter the BLT lattice and partially occupy the Ti-sites.

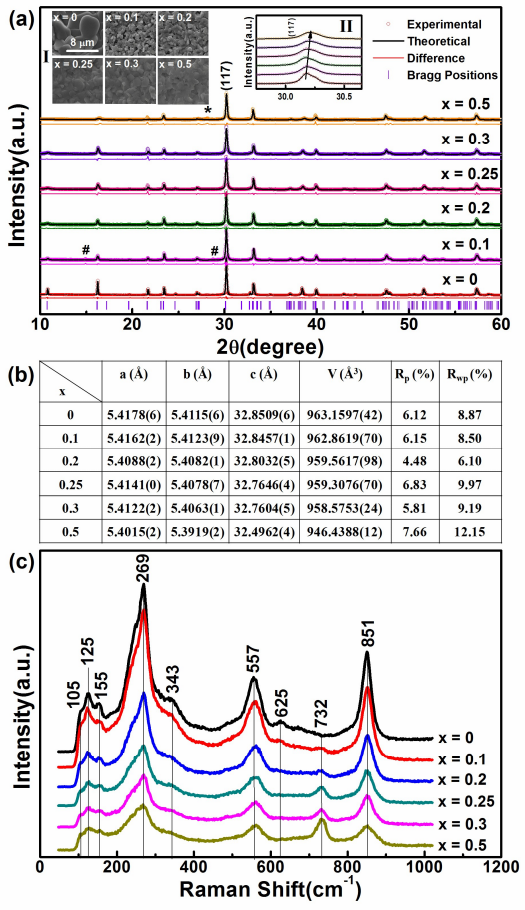

x	a (Å)	b (Å)	c (Å)	V (Å³)	R_p (%)	R_{wp} (%)
0	5.4178(6)	5.4115(6)	32.8509(6)	963.1597(42)	6.12	8.87
0.1	5.4162(2)	5.4123(9)	32.8457(1)	962.8619(70)	6.15	8.50
0.2	5.4088(2)	5.4082(1)	32.8032(5)	959.5617(98)	4.48	6.10
0.25	5.4141(0)	5.4078(7)	32.7646(4)	959.3076(70)	6.83	9.97
0.3	5.4122(2)	5.4063(1)	32.7604(5)	958.5753(24)	5.81	9.19
0.5	5.4015(2)	5.3919(2)	32.4962(4)	946.4388(12)	7.66	12.15

Fig. 1 (a) X-ray diffraction patterns of BLTFC ceramics (#: $Bi_2Ti_2O_7$, *: Bi_2O_3). Inset I gives surface morphologies of BLTFC ceramics, and inset II presents the amplified plot of the main diffraction peak (117). (b) Parameters obtained from Rietveld refinement. (c) Raman scattering spectra of BLTFC ceramics.

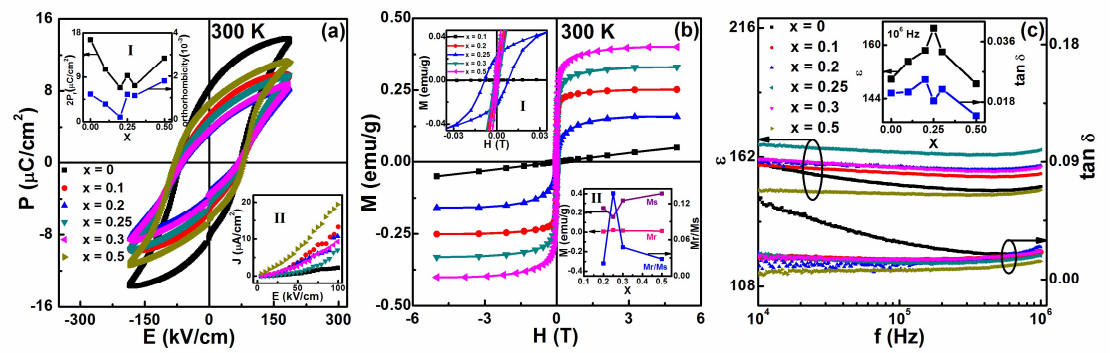

Fig. 2 (a) Room temperature *P-E* loops of BLTFC ceramics measured under applied electric field of 185 kV/cm and 100 Hz. Inset I shows the doping content dependent $2P_r$ and orthorhombicity, and inset II presents the leakage current characteristic. (b) Magnetic hysteresis loops of the BLTFC ($x \neq 0$) ceramics with the linear parts subtracted. Inset I shows the enlarged central part of the *M-H* curves, while inset II depict the doping content dependent M_r, M_s and M_r/M_s. (c) Frequency dependent dielectric constant (ε) and loss (tan δ) of BLTFC ceramics measured at room temperature. The inset shows the corresponding values for various doping content at 10^6 Hz.

The ferroelectric hysteresis (*P-E*) loops of BLTFC ceramics are measured under applied electric field of 185 kV/cm and 100 Hz at room temperature. As shown in Fig. 2(a), all the samples exhibit good ferroelectricity and typical *P-E* loops, with the remnant polarization ($2P_r$) of BLT (x = 0) being about 16.6 μC/cm^2, comparable to the reports.[20] Inset I of Fig. 2(a) shows $2P_r$ and the orthorhombicity of the samples, where the orthorhombicity, defined by 2(a - b)/(a + b)[19-21] as a measure of the orthorhombic distortion, is usually a reference for analyzing the ferroelectricity. It can be seen that the variations of $2P_r$ and orthorhombicity with the doping content are similar, but not entirely consistent. For samples with x > 0.25, although the orthorhombicity is comparable to that of the un-doped BLT ceramics, the $2P_r$ are obviously smaller. One of the possible origins is the smaller grain size of the doped samples compared with that of the un-doped BLT ceramics as mentioned above. It is known that, the variation in the grain size may be accompanied by the change in the domain configuration and domain wall mobility,[33] thus affecting the polarization switching. Note that, the small amount of impurity phases in the samples with x = 0.1 and 0.5 would cause uncertainty for the measurement of remnant polarization and the refined calculation of lattice parameters. Among the other doped samples, that with x = 0.25 possess the largest orthorhombicity and remnant polarization. Inset II of Fig. 2(a) presents the dc leakage current characteristic of BLTFC ceramics. The leakage current density of the x = 0.25 samples is lower than that with x = 0.2 and 0.3, which means the larger remnant polarization of the x = 0.25 ceramics is intrinsic, and not the contribution of leakage current.

The magnetic hysteresis (*M-H*) loops of the BLTFC ($x \neq 0$) ceramics are measured at room temperature (ESI Fig. S2).† In order to get a clearer image of ferromagnetic contribution in the *M-H* curves, the linear parts have been subtracted, which may come from the antiferromagnetic and paramagnetic contributions, and the results are shown in Fig. 2(b). Although the nearly linear *M-H* curve of the x = 0.1 sample indicates its non-ferromagnetic property, weak ferromagnetism is observed for all the other samples, which can be seen more clearly from inset I (the enlarged central parts of the *M-H* curves) of Fig. 2(b). Especially for the x = 0.25 sample, the *M-H* curve shows a significant hysteresis with remnant magnetization ($2M_r$) of about 0.043 emu/g and saturation magnetization (M_s) of about 0.158 emu/g. From inset II of Fig. 2(b), it can be seen that the x = 0.25 sample exhibits the largest remnant magnetization M_r and the smallest saturation magnetization M_s, and thus the biggest remnant magnetization ratio M_r/M_s, that is to say, the sample possesses the strongest ferromagnetism.

In this material system, ferromagnetism may be affected by the following factors: (1) Ferromagnetic interaction between bound magnetic polarons (BMPs).[22,23] In oxides, magnetic ions are easily to combine with oxygen vacancies forming BMPs, and the ferromagnetic interaction could arise with increasing concentration of the BMPs. (2) Ferromagnetic double exchange interaction between the non-equivalent Fe and Co ions.[13,14,24,25] According to the stoichiometric composition, Fe and Co ions mainly substitute for Ti^{4+} in the form of Fe^{3+} and Co^{3+}, and there might also be a small amount of divalent ions. Since the magnetic moments of the ions with either different kinds (Fe/Co) or different valences (+2/+3) are various, the ferromagnetic double exchange interaction can be formed between these adjacent ions through intermediate oxygen ions. Compared with single kind of magnetic ions, co-doping by two kinds of magnetic ions could greatly enhance the ferromagnetic double exchange interactions in the sample. (3) Antiferromagnetic

super exchange interaction between equivalent Fe or Co ions.[34] At lower doping concentration, the aforementioned non-equivalent magnetic ions have larger probability to be adjacent, while the probability of adjacent antiferromagnetic super exchange interaction between equivalent Fe or Co ions (such as Fe^{3+}-O^{2-}-Fe^{3+} or Co^{3+}-O^{2-}-Co^{3+}) increases with the increasing doping content.[35]

In addition, O 1s XPS spectra (ESI Fig. S1),† show that more oxygen vacancies present in the samples with x = 0.25, which might be associated with valences and substitution sites of Fe/Co ions. With the increase of doping content to more than x = 0.25, it might happen that a small amount of Fe^{3+}/Co^{3+} ions enter the Bi^{3+} sites, especially Bi is known to be volatile. In this case, oxygen vacancies could be less compared with the case of Ti^{4+} replacement.[36] In our samples, with increasing doping content, on the one hand, the concentration of oxygen vacancies increases, and the ferromagnetic interaction between BMPs associated with oxygen vacancies is enhanced; on the other hand, the ferromagnetic double exchange interaction between the non-equivalent Fe/Co ions is also strengthened. However, when x increases to more than 0.25, oxygen vacancies become less, and at the same time, the probability of adjacent antiferromagnetic super exchange interaction between equivalent Fe/Co ions increases, which finally results in larger remnant magnetization of the x = 0.25 samples.

Intriguingly, the x = 0.25 sample also possesses the largest dielectric constant at room temperature. As shown in Fig. 2(c), after doping, the variation of both the dielectric constant and loss with frequency are depressed, indicating the similar mechanisms dominating the dielectric response of the doped samples in the measuring frequency range. Especially, the x = 0.25 sample exhibits the largest dielectric constant while the relatively smaller dielectric loss at high frequency, which can be seen more clearly in the inset of Fig. 2(c).

Undoubtedly, the most important and common charged defects in oxides, which can respond to the small ac field for dielectric measurements, are oxygen vacancies. Figure 3 depicts the temperature dependent real part (M') and imaginary part (M") of dielectric modulus for BLTFC ceramics measured at various frequencies in the temperature range of 300-650 K. A dielectric anomaly is observed at the temperature range of 420-600 K for all the samples, and the peak locations of M" corresponding to the rapid decrease of M' move to higher temperature with increasing frequency, indicating typical dielectric relaxation behavior. According to the point defect relaxation theory, the activation energy E_a of relaxation units can be calculated by the Arrhenius law: $\tau = \tau_0 \exp(E_a / k_B T)$, where τ_0 is the relaxation time at an infinite temperature, k_B is the Boltzmann constant and T is the M"-peak temperature. The peak temperatures of M" at various frequencies are well fitted and shown in the insets of Fig. 3. The activation energies E_a are about 0.96, 0.92, 1.02, 1.07, 1.06 and

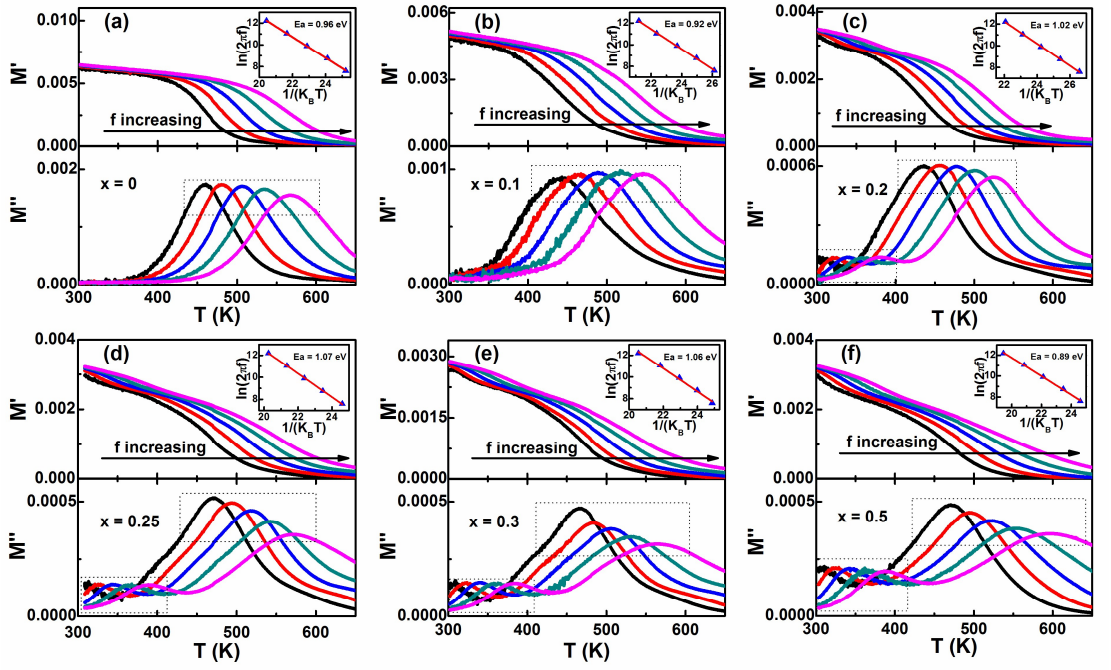

Fig. 3 Temperature dependent real part (M') and imaginary part (M") of dielectric modulus for BLTFC ceramics measured at various frequencies of $10^{2.5}$, 10^3, $10^{3.5}$, 10^4, and $10^{4.5}$ Hz. The insets give the relation between $\ln(2\pi f)$ and $1/k_BT$ according to the Arrhenius law for dielectric relaxation in the temperature range of 420-600 K.

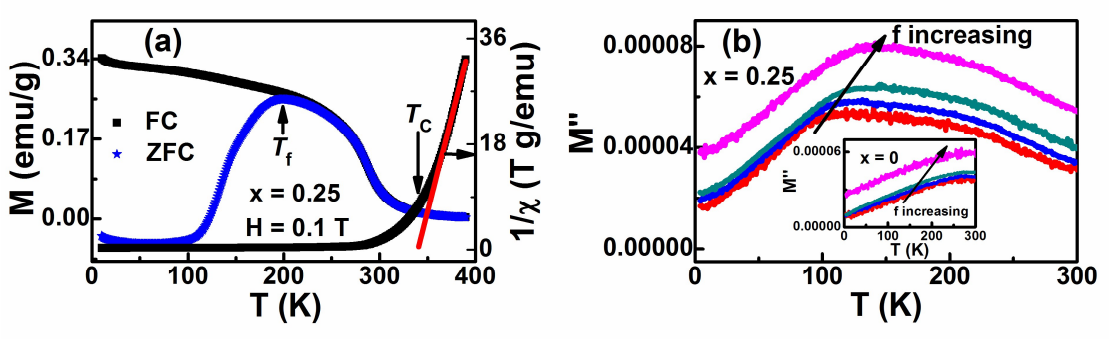

Fig. 4 (a) Magnetization and reverse magnetic susceptibilities as a function of temperature measured under ZFC and 0.1 T FC conditions for the x = 0.25 ceramic. (b) Imaginary part (M") of dielectric modulus for the x = 0.25 ceramic measured at low temperature and various frequencies of $10^{4.5}$, 10^5, $10^{5.5}$, and 10^6 Hz. The inset shows the corresponding M"-T curves for the BLT ceramic.

0.89 eV for the samples with x = 0, 0.1, 0.2, 0.25, 0.3 and 0.5, respectively, which are close to the migration energy of V_O^{2+} (each oxygen vacancy possessing two positive charges).[37,38] It can be seen that E_a of the x = 0.25 sample is slightly higher than that of the x = 0.2, 0.3 samples, showing lower mobility of oxygen vacancies. This result is consistent with the aforementioned dc leakage current. That is, the samples with x = 0.25 possess lower leakage current density under the same measuring electric field, indicating that the long range migration of charged defects (mainly oxygen vacancies) is more difficult.

So far, compared with the other two pure phase samples (x = 0.2, 0.3), it is found that the sample with x = 0.25 possesses greater remnant polarization, stronger ferromagnetism, larger room temperature dielectric constant, smaller room temperature dielectric loss, lower dc leakage current density, higher E_a while more oxygen vacancies. One of the above results seems to be contradictory with our previous works,[38-40] where the activation energy and the concentration of oxygen vacancies appeared to be inversely correlated for nonmagnetic-doped dielectric materials. However, for the magnetic-doped materials, the non-monotonic variation of the magnetic and electric response and the concentration of oxygen vacancies are not uncommon,[41-43] which may reflect the influence of magnetic interaction on the migration of charged defects.

Based on the above discussions, we believe that the magnetic and electric properties of the BLTFC ceramics should couple in a certain form. Figure 4(a) shows the temperature dependence of magnetization and reverse magnetic susceptibility ($1/\chi$) of the x = 0.25 sample, measured at 0.1 T after zero-field-cooling (ZFC) and then after field-cooling (FC) process. It is seen from the FC *M-T* curve that the sample undergoes a ferromagnetic to paramagnetic transition. According to the Curie-Weiss law: $\chi = C/(T - T_C)$, where C is the Curie constant, the extrapolated ferromagnetic Curie temperature T_C is about 340 K, far from those of potential contaminations, γ-Fe_2O_3 (900 K), Fe_3O_4 (850 K), Co_3O_4 (30 K) and $CoFe_2O_4$ (693 K).[5,44,45] Additionally, the broad line at g = 2.3 is absent in our Electron paramagnetic resonance (EPR) spectra at room temperature (ESI Fig. S3),† indicating that no Fe_2O_3 particle presents in our samples.[46,47] These facts, together with the above mentioned XRD and Raman scattering results, rule out the probability that the observed ferromagnetism in the x = 0.25 sample comes from the magnetic impurity phases. Moreover, the FC and ZFC *M-T* curves show typical irreversibility, and a hump appears in the ZFC *M-T* curve (the hump temperature T_f is about 199 K), indicating the possible spin glass behavior.[17] Figure 4(b) correspondingly shows the temperature dependent imaginary part (M") of dielectric modulus measured at low temperature. Combining Fig. 4(b) with the high temperature dielectric spectrum in Fig. 3(d), we can see two dielectric anomalies in the temperature range of 300-400 K and 100-220 K, which appear in the vicinity of the ferromagnetic Curie temperature T_C and spin glass freezing temperature T_f, respectively. Such dielectric anomalies also appear in other doped samples (ESI Fig. S4),† while it is not the case for BLT ceramics (Fig. 3(a) and the inset of Fig. 4(b)).

In the magnetoelectrically ordered systems, the dielectric anomaly near the magnetic transition temperature is considered as an effect of vanishing magnetic order.[48,49] Similar dielectric anomalies observed in $BiFeO_3$,[50,51] Fe or Mn doped $PbTiO_3$,[8-10] and $0.7Pb(Zr_{0.52}Ti_{0.48})O_3$-$0.3Pb(Ni_{1/3}Nb_{2/3})O_3$,[52] are attributed to the magnetoelectric coupling, however, their physical nature are unclear up to now. In our case, we believe that the dielectric anomalies probably come from the associated binding effect of magnetic

interaction on the migration of charged defects, especially oxygen vacancies. Unfortunately, no significant magnetodielectric effect is observed for our samples, which should be related to the aforementioned magnetoelectric coupling mechanism. Theoretical and experimental investigations are still needed to further explore the internal mechanism.

4. Conclusions

In summary, polycrystalline $Bi_{3.25}La_{0.75}(Ti_{3-x}Fe_{x/2}Co_{x/2})O_{12}$ ($0 \leq x \leq 0.5$) ceramics are successfully synthesized by conventional solid state reaction method, and the structural, multiferroic and dielectric properties are systematically characterized. Good ferroelectricity and weak ferromagnetism are obtained simultaneously at room temperature in the Fe/Co co-doped BLT ceramics when $x \geq 0.2$. The $x = 0.25$ samples possess the more prominent comprehensive properties with remnant polarization ($2P_r$) of about 9.3 μC/cm^2 and remnant magnetization ($2M_r$) of about 0.043 emu/g. Moreover, the dielectric anomalies appear near the ferromagnetic Curie temperature T_C and the spin glass freezing temperature T_f, exhibiting magnetoelectric coupling behavior, which may result from the associated binding effect of magnetic interaction on the migration of charged defects, especially oxygen vacancies. The present work highlights the possibility of Fe/Co co-doped BLT as a potential room temperature multiferroics.

Acknowledgements

This work was supported by National Natural Science Foundation of China (Nos. 51225201 and 61271078), the 973 Project of MOST (No. 2015CB921201), the Priority Academic Program Development of Jiangsu Higher Education Institutions (PAPD) and the Fundamental Research Funds for the Central Universities.

Notes and references

1. H. Zheng, J. Wang, S. E. Lofland, Z. Ma, L. Mohaddes-Ardabili, T. Zhao, L. Salamanca-Riba, S. R. Shinde, S. B. Ogale, F. Bai, D. Viehland, Y. Jia, D. G. Schlom, M. Wuttig, A. Roytburd and R. Ramesh, *Science*, 2004, 303, 661-663.
2. W. Eerenstein, N. D. Mathur and J. F. Scott, *Nature*, 2006, 442, 759-765.
3. S. W. Cheong and M. Mostovoy, *Nat. Mater.*, 2007, 6, 13-20.
4. R. Ramesh and N. A. Spaldin, *Nat. Mater.*, 2007, 6, 21-29.
5. B. Xu, K. B. Yin, J. Lin, Y. D. Xia, X. G. Wan, J. Yin, X. J. Bai, J. Du and Z. G. Liu, *Phys. Rev. B*, 2009, 79, 134109.
6. Y. H. Lin, J. C. Yuan, S. Y. Zhang, Y. Zhang, J. Liu, Y. Wang and C. W. Nan, *Appl. Phys. Lett.*, 2009, 95, 033105.
7. G. S. Gong, Y. J. Fang, G. Zerihun, C. Y. Yin, S. Huang and S. L. Yuan, *J. Appl. Phys.*, 2014, 115, 243902.
8. V. R. Palkar and S. K. Malik, *Solid State Commun.*, 2005, 134, 783-786.
9. M. Kumar and K. L. Yadav, *J. Phys.: Condens. Matter*, 2007, 19, 242202.
10. F. Craciun, E. Dimitriu, M. Grigoras and N. Lupu, *Appl. Phys. Lett.*, 2013, 102, 242903.
11. X. W. Dong, K. F. Wang, J. G. Wan, J. S. Zhu and J. M. Liu, *J. Appl. Phys.*, 2008, 103, 094101.
12. H. Y. Zhao, H. Kimura, Z. X. Cheng, M. Osada, J. L. Wang, X. L. Wang, S. X. Dou, Y. Liu, J. D. Yu, T. Matsumoto, T. Tohei, N. Shibata and Y. Ikuhara, *Sci. Rep.*, 2014, 4, 5255.
13. X. Y. Mao, W. Wang, X. B. Chen and Y. L. Lu, *Appl. Phys. Lett.*, 2009, 95, 082901.
14. X. Y. Mao, H. Sun, W. Wang, Y. L. Lu and X. B. Chen, *Solid State Commun.*, 2012, 152, 483-487.
15. F. Z. Huang, X. M. Lu, T. T. Xu, Y. Y. Liu, W. N. Su, Y. M. Jin, Y. Kan and J. S. Zhu, *Thin Solid Films*, 2012, 520, 6489-6492.
16. X. Y. Mao, H. Sun, W. Wang, X. B. Chen and Y. L. Lu, *Appl. Phys. Lett.*, 2013, 102, 072904.
17. B. Yuan, J. Yang, J. Chen, X. Z. Zuo, L. H. Yin, X. W. Tang, X. B. Zhu, J. M. Dai, W. H. Song and Y. P. Sun, *Appl. Phys. Lett.*, 2014, 104, 062413.
18. B. H. Park, B. S. Kang, S. D. Bu, T. W. Noh, J. Lee and W. Joe, *Nature*, 1999, 401, 682-684.
19. Y. Shimakawa, Y. Kubo, Y. Tauchi, H. Asano, T. Kamiyama, F. Izumi and Z. Hiroi, *Appl. Phys. Lett.*, 2001, 79, 2791.
20. M. K. Jeon, Y. I. Kim, J. M. Sohn and S. I. Woo, *J. Phys. D: Appl. Phys.*, 2004, 37, 2588-2592.
21. S. J. Kim, C. Moriyoshi, S. Kimura, Y. Kuroiwa, K. Kato, M. Takata, Y. Noguchi and M. Miyayama, *Appl. Phys. Lett.*, 2007, 91, 062913.
22. X. Q. Chen, F. J. Yang, W. Q. Cao, D. Y. Wang and K. Chen, *J. Phys. D: Appl. Phys.*, 2010, 43, 065001.
23. J. Paul, S. Bhardwaj, K. K. Sharma, R. K. Kotnala and R. Kumar, *J. Alloy. Compd.*, 2015, 634, 58-64.
24. X. Q. Chen, C. Wei, J. Xiao, Y. Xue, X. B. Zeng, F. J. Yang, P. Li and Y. B. He, *J. Phys. D: Appl. Phys.*, 2013, 46, 425001.
25. J. Paul, S. Bhardwaj, K. K. Sharma, R. K. Kotnala and R. Kumar, *J. Mater. Sci.*, 2014, 49, 6056-6066.
26. J. F. Dorrian, R. E. Newnham, M. I. Kay and D. K. Smith, *Ferroelectrics*, 1972, 3, 17-27.
27. R. D. Shannon, *Acta Crystallogr. Sec. A*, 1976, 32, 751-767.
28. S. Kojima, R. Imaizumi, S. Hamazaki and M. Takashige, *Jpn. J. Appl. Phys.*, 1994, 33, 5559-5564.
29. P. R. Graves, G. Hua, S. Myhra and J. G. Thompson, *J. Solid State Chem.*, 1995, 114, 112-122.
30. D. L. A. Faria, S. V. Silva and M. T. Oliveira, *J. Raman Spectrosc.*, 1997, 28, 873-878.
31. D. Gallant, M. Pézolet, and S. Simard. *J. Phys. Chem. B*, 2006, 110, 6871-6880.
32. T. Yu, Z. X. Shen and J. Ding, *J. Phys.: Condens. Matter*, 2002, 14, L613-L618.
33. C. A. Randall, N. Kim, J. P. Kucera, W. Cao and T. R. Shrout, *J. Am. Ceram. Soc.*, 1998, 81, 677-688.
34. J. He, X. M. Lu, W. L. Zhu, Y. Y. Hou, R. X. Ti, F. Z. Huang, X. L. Lu, T. T. Xu, J. Su and J. S. Zhu,

Appl. Phys. Lett., 2015, 107, 012409.
35. H. S. Kim, L. Bi, G. F. Dionne and C. A. Ross, *Appl. Phys. Lett.*, 2008, 93, 092506.
36. H. R. Wu, F. Z. Huang, T. T. Xu, R. X. Ti, X. M. Lu, Y. Kan, X. L. Lv, W. L. Zhu and J. S. Zhu, *J. Appl. Phys.*, 2015, 117, 144101.
37. J. F. Scott and M. Dawber, *Appl. Phys. Lett.*, 2000, 76, 3801.
38. Y. Y. Yao, C. H. Song, P. Bao, D. Su, X. M. Lu, J. S. Zhu and Y. N. Wang, *J. Appl. Phys.*, 2004, 95, 3126.
39. W. Li, J. Gu, C. H. Song, D. Su and J. S. Zhu, *J. Appl. Phys.*, 2005, 98, 114104.
40. M. F. Zhang, Y. Wang, K. F. Wang, J. S. Zhu and J. M. Liu, *J. Appl. Phys.*, 2009, 105, 061639.
41. T. S. Herng, M. F. Wong, D. C. Qi, J. B. Yi, A. Kumar, A. Huang, F. C. Kartawidjaja, S. Smadici, P. Abbamonte, C. S. Hanke, S. Shannigrahi, J. M. Xue, J. Wang, Y. P. Feng, A. Rusydi, K. Y. Zeng and J. Ding, *Adv. Mater.*, 2011, 23, 1635-1640.
42. B. N. Khare, M. J. Kappers, M. Wei, M. G. Blamire and J. L. M. M. Driscoll, *Adv. Mater.*, 2006, 18, 1449-1452.
43. Y. K. An, S. Q. Wang, L. S. Duan, J. W. Liu and Z. H. Wu, *Appl. Phys. Lett.*, 2013, 102, 212411.
44. Y. Ikedo, J. Sugiyama, H. Nozaki, H. Itahara, J. H. Brewer, E. J. Ansaldo, G. D. Morris, D. Andreica and A. Amato, *Phys. Rev. B*, 2007, 75, 054424.
45. K. C. Verma, V. P. Singh, M. Ram, J. Shah and R. K. Kotnala, *J. Magn. Magn. Mater.*, 2011, 323, 3271-3275.
46. R. Singh, *J. Phys. D: Appl. Phys.*, 1984, 17, L57-L60.
47. M. Devadas, O. Kröcher, M. Elsener, A. Wokaun, G. Mitrikas, N. Söger, M. Pfeifer, Y. Demel and L. Mussmann, *Catal. Today*, 2007, 119, 137-144.
48. T. Kimura, S. Kawamoto, I. Yamada, M. Azuma, M. Takano and Y. Tokura, *Phys. Rev. B*, 2003, 67, 180401.
49. K. F. Wang, J. M. Liu and Z. F. Ren, *Adv. Phys.*, 2009, 4, 321-448.
50. R. Mazumder, S. Ghosh, P. Mondal, D. Bhattacharya, S. Dasgupta, N. Das, A. Sen, A. K. Tyagi, M. Sivakumar, T. Takami and H. Ikuta, *J. Appl. Phys.*, 2006, 100, 033908.
51. F. Z. Huang, X. M. Lu, W. W. Lin, W. Cai, X. M. Wu, Y. Kan, H. Sang and J. S. Zhu, *Appl. Phys. Lett.*, 2007, 90, 252903.
52. J. Su, X. M. Lu, Y. Y. Liu, J. T. Zhang, G. R. Li, X. Z. Ruan, F. Z. Huang, J. Du and J. S. Zhu, *Appl. Phys. Lett.*, 2012, 100, 102905.

Highlight:

Good ferroelectricity, weak ferromagnetism and the sign of magnetoelectric coupling are obtained simultaneously in $Bi_{3.25}La_{0.75}(Ti_{2.75}Fe_{0.125}Co_{0.125})O_{12}$ ceramics.